Nucleic Acids Research, 2025, **53**, gkaf618
https://doi.org/10.1093/nar/gkaf618
RNA and RNA-protein complexes

Distant ribose 2′-*O*-methylation of 23S rRNA helix 69 pre-orders the capreomycin drug binding pocket at the ribosome subunit interface

Suparno Nandi [1], Debayan Dey [1], Pooja Srinivas [2,3], Christine M. Dunham [2,4], Graeme L. Conn [1,4,*]

[1]Department of Biochemistry, Emory University School of Medicine, Atlanta, GA 30322, United States
[2]Department of Chemistry, Emory University, Atlanta, GA 30322, United States
[3]Graduate Program in Molecular and Systems Pharmacology, Emory University, Atlanta, GA 30322, United States
[4]Emory Antibiotic Resistance Center (ARC), Emory University, Atlanta, GA 30322, United States
[*]To whom correspondence should be addressed. Email: gconn@emory.edu

Abstract

Loss of ribosomal RNA (rRNA) modifications incorporated by the intrinsic methyltransferase TlyA results in reduced sensitivity to tuberactinomycin antibiotics such as capreomycin. However, how rRNA methylation alters drug binding, particularly at the distant but functionally more important site in 23S rRNA helix 69 (H69), is currently unknown. We determined high-resolution cryo-electron microscopy structures of the *Mycolicibacterium smegmatis* 70S ribosome with or without the two ribose 2′-*O*-methyl modifications incorporated by TlyA. In the unmodified ribosome, the tip of H69 adopts a more compact conformation, positioning two key nucleotides (A2137 and C2138) such that interactions with capreomycin would be lost and the binding pocket partially occluded. Methylation of 23S rRNA nucleotide C2144 promotes conformational changes that result in a more favorable positioning of C2138 and adoption of a more open conformation to enable capreomycin binding. Molecular dynamics simulations and H69 RNA helical analyses additionally reveal specific propagation of these changes from the site of modification to the H69 tip, allosterically reconfiguring the capreomycin binding site. Methylation of h44 also results in structural rearrangements at the H69–h44 interface to support maintenance of these changes that favor antibiotic binding. This work thus reveals the effect and regulation of distant rRNA methylation on ribosome-targeting antibiotic binding.

Graphical abstract

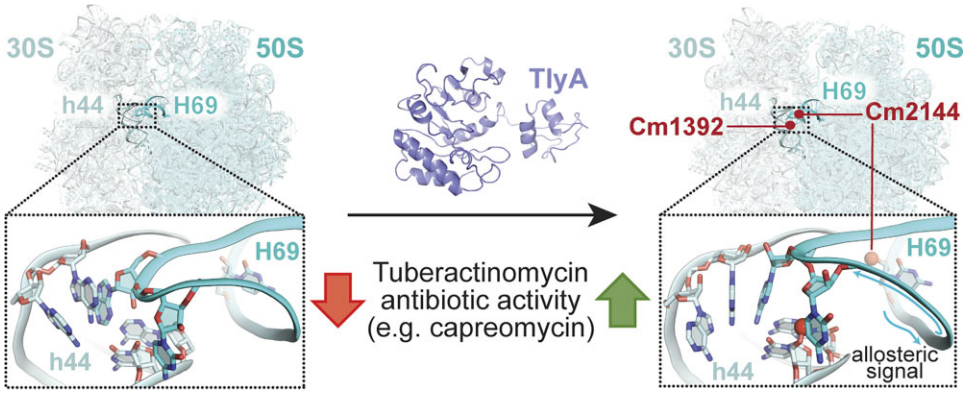

Introduction

Ribosome-targeting antibiotics have been critical for our ability to treat bacterial infections, but these essential drugs are now threatened by multiple resistance mechanisms [1]. One major mode of resistance is conferred by antibiotic-resistance *S*-adenosyl-L-methionine (SAM)-dependent ribosomal RNA (rRNA) methyltransferases [2]. For example, 23S rRNA methyltransferases of the Erm family are a clinically prevalent mechanism of resistance to macrolide antibiotics, while more recently, the aminoglycoside-resistance 16S rRNA methyltransferases have emerged as a new threat to even the most recently approved aminoglycoside antibiotics [3–5].

In contrast to these methyltransferases that confer antibiotic resistance by introducing rRNA modifications, loss

Received: November 5, 2024. **Revised:** May 23, 2025. **Editorial Decision:** June 11, 2025. **Accepted:** June 13, 2025
© The Author(s) 2025. Published by Oxford University Press on behalf of Nucleic Acids Research.
This is an Open Access article distributed under the terms of the Creative Commons Attribution-NonCommercial License (https://creativecommons.org/licenses/by-nc/4.0/), which permits non-commercial re-use, distribution, and reproduction in any medium, provided the original work is properly cited. For commercial re-use, please contact reprints@oup.com for reprints and translation rights for reprints. All other permissions can be obtained through our RightsLink service via the Permissions link on the article page on our site—for further information please contact journals.permissions@oup.com.

Downloaded from https://academic.oup.com/nar/article/53/13/gkaf618/8192813 by Acquisitions Dept Serials user on 23 July 2025

of intrinsic rRNA methylation can also result in reduced antibiotic efficacy. For instance, deletion of the 16S rRNA methyltransferases RsmA (formerly KsgA) [6] or RsmG [7] reduces susceptibility to the antibiotics kasugamycin and streptomycin, respectively. Similarly, loss of the cytidine-2′-*O*-methyltransferase TlyA results in decreased susceptibility to tuberactinomycin antibiotics such as capreomycin and viomycin [8]. TlyA is encoded by all mycobacterial species, including the causative agent of tuberculosis (TB), *Mycobacterium tuberculosis* (*Mtb*), and loss of the rRNA modifications incorporated by TlyA results in clinical resistance to capreomycin, a drug previously used for treating multidrug-resistant TB [9, 10].

TlyA enzymes act on individual ribosomal subunits (30S or 50S) and are divided into two subgroups that incorporate either a single ribose modification in 23S rRNA of the large subunit (Type I) or two ribose modifications via dual 16S/23S rRNA activity (Type II). Mycobacterial species, including *Mtb* and *Mycolicibacterium smegmatis* (*Msm*), encode Type II enzymes ($TlyA^{II}$) and thus have ribosomes modified with Cm2144 on 23S rRNA Helix 69 (H69) and Cm1392 on 16S rRNA helix 44 (h44). Note that, hereafter, the terms methylated and unmethylated ribosomes are used to denote the presence or absence of $TlyA^{II}$-mediated dual methylation and *Msm* nucleotide numbering is used unless otherwise indicated (numbering conversion for nucleotides from other bacteria discussed in the text is provided in Table 1). Notably, single modification of Cm2144 via expression of *Thermus thermophilus* (*Tth*) Type I TlyA in *Escherichia coli* (*Eco*; which lacks TlyA) resulted in a four-fold increase in sensitivity to both capreomycin and viomycin, whereas dual methylation via expression of *Msm* Type II TlyA further increased only viomycin susceptibility (by two-fold more). These findings indicate that the H69 Cm2144 modification makes the major relative contribution to tuberactinomycin activity despite its greater distance (~20 Å) from the drug binding site [11]. X-ray crystallographic and single-particle cryo-electron microscopic (cryo-EM) structures of the *Mtb* [12], *Tth* [13], and *Msm* [14] 70S ribosomes with capreomycin show that the antibiotic binds at the subunit interface created by H69 and h44, adjacent to the aminoacyl (A) site. Antibiotic binding at the H69–h44 interface has been proposed to alter the position of several H69 and h44 nucleotides and thus their interactions with the A-site tRNA, inhibiting the decoding step and/or tRNA translocation [1, 13, 15].

While the necessity of rRNA methylation for optimal capreomycin binding to mycobacterial ribosomes is well documented, the molecular mechanism by which these modifications facilitate the drug–rRNA interaction is unclear. Methylated 16S rRNA C1392 is located at the drug binding pocket, but as this residue appears to form only weak hydrogen bonds (>4 Å) with capreomycin [8, 14, 16], its modification cannot directly impact antibiotic binding. In structures of ribosomes from *Staphylococcus aureus* [17] and *Listeria innocua* [18] that lack TlyA and thus its associated methylations, the tip of H69 moves toward h44, adopting a more compact conformation with the H69 nucleobases oriented away from the drug binding pocket. In contrast, in $TlyA^{II}$-modified *Msm* ribosomes without capreomycin, the phosphate backbone of the H69 tip (nucleotides A2136–U2139) shifts away from h44 by ~3 Å, repositioning the nucleobases of H69 to face the capreomycin binding pocket [14]. From these observations, we and others [8, 11, 19] speculated that the more compact conformation of H69 somehow results from the lack of both modifications deposited by $TlyA^{II}$, and results in greater occlusion of the capreomycin binding pocket. In contrast, H69 rRNA methylation, and the altered H69 conformation that results, could favor interaction with capreomycin resulting in the observed rRNA modification-dependent sensitivity to the drug.

Table 1. Numbering of 23S (H69) and 16S (h44) rRNA nucleotides discussed in this work

rRNA	*Msm*[a]	*Mtb*	*Eco*/*Tth*[b]
23S rRNA H69	2129	2143	1905
	2130	2144	1906
	2131	2145	1907
	2132	2146	1908
	2133	2147	1909
	2134	2148	1910
	2135	2149	1911
	2136	2150	1912
	2137	2151	1913
	2138	2152	1914
	2139	2153	1915
	2140	2154	1916
	2141	2155	1917
	2142	2156	1918
	2143	2157	1919
	2144[c]	2158[c]	1920[c]
	2145	2159	1921
	2146	2160	1922
	2147	2161	1923
	2148	2162	1924
16S rRNA h44 (5′)	1392[c]	1402[c]	1409
	1391	1401	1408
16S rRNA h44 (3′)	1477	1486	1493
	1476	1485	1492
	1475	1484	1491

[a] *Msm* numbering is used in the text.
[b] *Tth* crystal structures use conversion to *Eco* numbering.
[c] Sites of Tly^{II} 2′-*O*-methyl modification.

Here, we report high-resolution cryo-EM structures of the *Msm* 70S ribosome with and without the two rRNA modifications incorporated by $TlyA^{II}$. These structures and complementary molecular dynamics (MD) simulations reveal the critical role of C2144 methylation and propagation of its effect on the RNA helical structure of H69, including allosteric changes produced at the distant drug binding pocket at the tip of H69. In addition, our findings suggest a role for C1392 methylation in maintaining the more open H69 conformation and the overall architecture of the capreomycin binding pocket in the absence of the drug. RNA modifications that mediate allosteric changes in antibiotic binding sites, such as those revealed here for the tuberactinomycin antibiotics, thus represent an important new consideration for designing more effective small molecules targeting the bacterial ribosome.

Materials and methods

Purification of *Msm* 70S ribosomes

Ribosomes were isolated from *Msm* strains with (LR222) or without (LR222 C101A) $TlyA^{II}$, as reported previously [20]. Briefly, single colonies of *Msm* LR222 or LR222 C101A were used to inoculate 20 ml Middlebrook 7H9 liquid medium and grown overnight at 37°C with mild agitation (shaking at 100 rpm). Fresh Middlebrook 7H9 medium (1–2 l) was inoculated

Downloaded from https://academic.oup.com/nar/article/53/13/gkaf618/8192813 by Acquisitions Dept Serials user on 23 July 2025

with the overnight culture (1:100 dilution), and the cultures were grown at 37°C with mild agitation over 35–41 h to an OD_{600} of ∼4.0. Cells were collected by centrifugation at 4000 × *g* for 10 min at 4°C, washed twice (500 ml/l culture) with Buffer 1 (10 mM HEPES/KOH, pH 7.6, 1 M NH_4Cl, 10 mM $MgCl_2$, and 6 mM β-mercaptoethanol), and then once with the same buffer but with 0.1 M NH_4Cl (Buffer 2).

Cells were resuspended in 5 ml of Buffer 2 per g of wet cell mass and lysed by two passes through an EmulsiFlex-C5 high-pressure homogenizer (Avestin). After adding DNase I (10 U/ml lysate), the lysate was cleared by centrifugation for 10 and 20 min at 19 400 × *g* and 27 000 × *g*, respectively. Ribosomes were pelleted by ultra-high-speed centrifugation of the supernatant at 278 800 × *g* for 18 h. To remove bound tRNA, ribosome subunits were split by resuspension and dialysis against Buffer 3 (10 mM HEPES/KOH, pH 7.6, 0.1 M NH_4Cl, 0.3 mM $MgCl_2$, and 6 mM β-mercaptoethanol), followed by reassociation via subsequent overnight dialysis against Buffer 2. Reassembled 70S ribosomes were separated from individual subunits by centrifugation (90 200 × *g*) on a 10%–40% sucrose gradient for 18 h at 4°C, and subsequent fractionation using an ÄKTA Purifier10 system. Pooled 70S fractions were centrifuged at 226 000 × *g* for 18 h at 4°C and the pelleted 70S resuspended, dialyzed overnight against Buffer 2, and flash-frozen for storage at −80°C as 20 μl aliquots of LR222 (2.55 μM) and LR222 C101A (2.39 μM).

Cryo-EM specimen preparation, data collection, and structure determination

Ribosomes were diluted to 1.0 and 3.0 μM for LR222 (TlyA-methylated) and LR222 C101A, respectively. Each sample (3 μl) was applied to glow-discharged Quantifoil Cu R1.2/1.3 300 mesh grids, blotted for 4 s, and, after a 10 s wait time, vitrified in liquid ethane using a Vitrobot Mark IV (Thermo Fisher Scientific) operating at 4°C and 100% relative humidity.

Cryo-EM micrographs (5060 and 5665 for LR222 and LR222 C101A, respectively) were recorded as movies using Leginon [21] with defocus range of −0.6 to −2.2 μm and −0.6 to −2.1 μm at 81 000× magnification (1.069 Å/pixel) on a Titan Krios 300 kV microscope with a Gatan K3 direct electron detector at the National Center for CryoEM Access and Training. The total dose was 52.51 $e^-/Å^2$, distributed over 40 frames for 2.0 s (50 ms per frame), resulting in a dose rate of 1.31 $e^-/Å$ per frame.

The complete workflow for cryo-EM structure determination is summarized in Supplementary Figs S1 and S2. First, aligned and dose-weighted images were imported, and the contrast transfer function (CTF) estimate was accomplished using Gctf in RELION 3.1 [22, 23]. Automated particle picking was guided by an initial Laplacian-of-Gaussian-based autopicking of 200 images, which resulted in 35 443 and 42 841 particles for LR222 and LR222 C101A, respectively. Two-dimensional (2D) classes of these particles were used as a reference for subsequent autopicking with each complete image dataset, resulting in the selection of 3 878 842 and 4 579 196 particles (400-pixel box size, 1.069 Å/pixel), respectively, which were 4 × 4 binned (100-pixel box size, 4.276 Å/pixel). Following the 2D classification of each particle set, an initial map was created from the classes and used to generate 3D maps by iterative rounds of 3D refinement and 3D classification to remove non-ribosomal particles. The particles corresponding to the final 3D classes for both reconstructions were then unbinned at full resolution (400-pixel box size, 1.069 Å/pixel), and following a final round of 3D classification to remove unsuitable classes for the non-TlyA methylated ribosome, multiple rounds of 3D and CTF refinements resulted in postprocessed maps of 3.17 and 3.24 Å for LR222 (TlyA methylated) and LR222 C101A (non-methylated) ribosomes, respectively.

To improve the resolution of the maps, multibody refinement [24] was also performed on the final selected particles with individual masks corresponding to the large and small subunits of each ribosome. This process resulted in four maps with resolutions of 3.08 Å (50S) and 3.19 Å (30S) for LR222, and 3.17 Å (50S) and 3.34 Å (30S) for LR222 C101A. Postprocessing of these maps without sharpening did not result in further enhancement of resolution based on gold-standard refinement Fourier shell correlation (0.143 cut-off) (Supplementary Fig. S3A–C and G–I). The postprocessed maps were subsequently sharpened using PHENIX (adjusted surface area) [25]. Additionally, DeepEMhancer [26] was used to sharpen the half-maps obtained from multibody refinement of the individual subunits in both methylated and unmethylated ribosomes. Relion-3.1 was used to generate local resolution maps (Supplementary Fig. S3D–F and J–L).

The 3D refined map was used to build the initial model for both the methylated and unmethylated ribosomes. An *Msm* 70S structure (PDB code 5ZEB) without tRNA was docked in the map for each ribosome and refined using global minimization, rigid body, local grid search, simulated annealing, and *B*-factor refinement in PHENIX [27]. Subsequently, each 70S model was split into individual 50S and 30S subunits, and each docked in its corresponding multibody refined map using Chimera (v1.16) [28]. Each subunit model was further refined using the same strategies in PHENIX. Finally, the individual subunit models were merged to create a final complete model of 70S followed by final model adjustment in COOT (v0.9.8.1) using the DeepEMhancer sharpened multibody refinement maps for each subunit [29]. Both structures were validated using PHENIX, and the final parameters for data collection, processing, model construction, refinement, and validation are provided in Table 2. Structural images were prepared using PyMOL (v2.5.4) [30] or ChimeraX (v1.7) [31] using the DeepEMhancer sharpened multibody refinement maps for each subunit.

MD simulations

MD simulations were performed using two different sets of coordinates prepared in both methylated and unmethylated states: System 1—extracted from the capreomycin-bound *Mtb* 70S ribosome (PDB code 5V93) and comprising select 23S rRNA (chain A; H69 nucleotides 2144–2162^{Mtb}), 16S rRNA (chain a; nucleotides 12–28^{Mtb}, 490–537^{Mtb}, 769–789^{Mtb}, 847–926^{Mtb}, 1377–1409^{Mtb}, and 1476–1514^{Mtb}), ribosomal protein S12 (chain l), a mitochondrial domain of uncharacterized function protein (chain x), and capreomycin, as previously described [32]. Methyl groups were added to both 23S rRNA $C2158^{Mtb}$ (C2144) and 16S rRNA $C1402^{Mtb}$ (C1392) to generate the methylated System 1, as these modifications were not modeled in the original structure. System 2—a 19-nucleotide segment of 23S rRNA H69 (nucleotides 2129–2148) extracted directly from our methylated and unmethylated *Msm* 70S ribosome structures.

Downloaded from https://academic.oup.com/nar/article/53/13/gkaf618/8192813 by Acquisitions Dept Serials user on 23 July 2025

Table 2. Cryo-EM data collection, refinement, and model validation for the methylated and unmethylated *M. smegmatis* 70S ribosome

	LR222 (methylated)			LR222 C101A (unmethylated)		
		Multibody refinement			Multibody refinement	
	70S	50S	30S	70S	50S	30S
Coordinates (PDB)	9E0P			9E0N		
Map (EMDB)	47365			47363		
Data collection/processing						
Microscope	TFS Titan Krios			TFS Titan Krios		
Camera	Gatan K3			Gatan K3		
Voltage (kV)	300			300		
Magnification	81 000×			81 000×		
Electron exposure ($e^-/Å^2$)	52.51			52.51		
Defocus range	−0.6 to −2.2			−0.6 to −2.1		
Pixel size (Å)	1.069			1.069		
Symmetry	C1			C1		
No. of particles, initial	3 878 842			4 579 196		
final	443 500			227 969		
Map resolution (FSC 0.143) (Å)[a]	3.17/3.50	3.08/3.08	3.19/3.19	3.24/3.59	3.19/3.17	3.37/3.34
Refinement and model						
Model resolution (Å)[a] (FSC 0.143, unmasked)	3.0/3.1	2.9/2.7	3.1/3.2	3.1/3.0	3.1/3.1	3.2/3.1
CC_{mask}[a]	0.78/0.76	0.83/0.83	0.73/0.74	0.73/0.75	0.67/0.68	0.70/0.71
Non-hydrogen atoms						
Protein residues	6095	3689	2406	6095	3689	2406
RNA residues	4725	3219	1506	4725	3219	1506
Ligand/modified nucleotide	139	114	24	107	79	28
B-factors (min./max./mean) ($Å^2$)						
Protein	30/999.9/259.4	30/999.9/178.5	84.4/999.9/379.7	67.27/734.2/183.7	67.27/734.2/136.2	104.4/613.3/254.4
RNA	20/999.9/241.9	65.1/999.9/185.3	20.0/999.9/362.7	68.4/999.9/175.9	68.4/999.9/147.7	105.6/999.9/236.4
Ligand/modified nucleotide	30/999.9/126.8	53.2/275.6/85.6	85.6/ 999.9/326.7	50.9/582.3/113.7	50.9/114.5/77.3	93.8/582.3/210.7
RMS deviations						
Bond lengths (Å)	0.002	0.002	0.003	0.002	0.002	0.002
Bond angles (°)	0.606	0.558	0.69	0.603	0.55	0.694
Validation						
MolProbity score	1.63	1.75	1.76	1.70	1.79	1.84
Clashscore	5.5	7.67	7.69	6.42	8.33	8.91
Rotamer outliers (%)	0.59	0.75	0.35	0.75	0.61	0.95
Ramachandran plot (protein)						
Favored (%)	95.21	95.25	95.14	94.98	95.14	94.72
Allowed (%)	4.79	4.75	4.86	5.01	4.83	5.28
Disallowed (%)	0.00	0.00	0.00	0.02	0.03	0.00

[a]Values shown are the resolution for postprocess/3D refinement maps.

To make these simulations computationally feasible while preserving essential structural context, we employed a "restrained ribosomal section approach," in which specific contiguous regions of the ribosome were isolated and restraints applied to peripheral atoms to mimic those normally imposed by surrounding residues. Importantly, the site of interest and its associated ligands were left fully unrestrained to allow unbiased sampling of local dynamics. For System 1, a weak positional restraint ($k = 0.5$) was applied to regions surrounding H69 (i.e. 16S rRNA and the two ribosomal proteins) and the two nucleotides on each end of H69. No restraints were applied to the remainder of H69 or capreomycin. For System 2, a positional restraint ($k = 1$) was applied to the terminal nucleotides (2129–2131 and 2147–2148) of *Msm* H69 to maintain structural stability. Partially restrained classical MD simulations for both systems were performed using Desmond from the Schrödinger software (2023-4) with the OPLS4 force field, which accommodates modified RNA residues. Prior to simulation, each system was neutralized by adding Na^+ ions in the Schrödinger software System Builder module. Neutralized systems were then immersed in TIP3P water and random water molecules replaced with Na^+ ions to achieve a total ionic strength of 150 mM NaCl. Each fully solvated and neutralized system then underwent relaxation and equilibration in the isobaric–isothermal (NPT) ensemble ($P = 1$ atm, $T = 310$ K) for 10 ns (System 1) or 30 ns (System 2). Subsequently, replicate production simulations (3×100 ns) were conducted using the Nose–Hoover chain and Martyna–Tobias–Klein thermostat and barostat with relaxation times of 1 and 2 ps, respectively, in the canonical (NPT) ensemble using the last configuration from equilibration. The equations of motion were integrated using multiple time steps for short-range (2 fs) and long-range (6 fs) interactions with a 9-Å cutoff for nonbonded interactions. Coordinates were saved every 100 ps.

For System 1, the effect of methylation on the overall dynamics of H69 was assessed using root-mean-square fluctuation (RMSF) differences. Specific conformational changes at the tip of H69 were also evaluated by measuring the angle between $A2151^{Mtb}$ (A2137) and $C2152^{Mtb}$ (C2138), calculated using the adenine N1, cytidine N9, and the phosphate linking the two nucleotides. The binding affinity of capreomycin to the RNA (H69 and h44 combined) was assessed

Downloaded from https://academic.oup.com/nar/article/53/13/gkaf618/8192813 by Acquisitions Dept Serials user on 23 July 2025

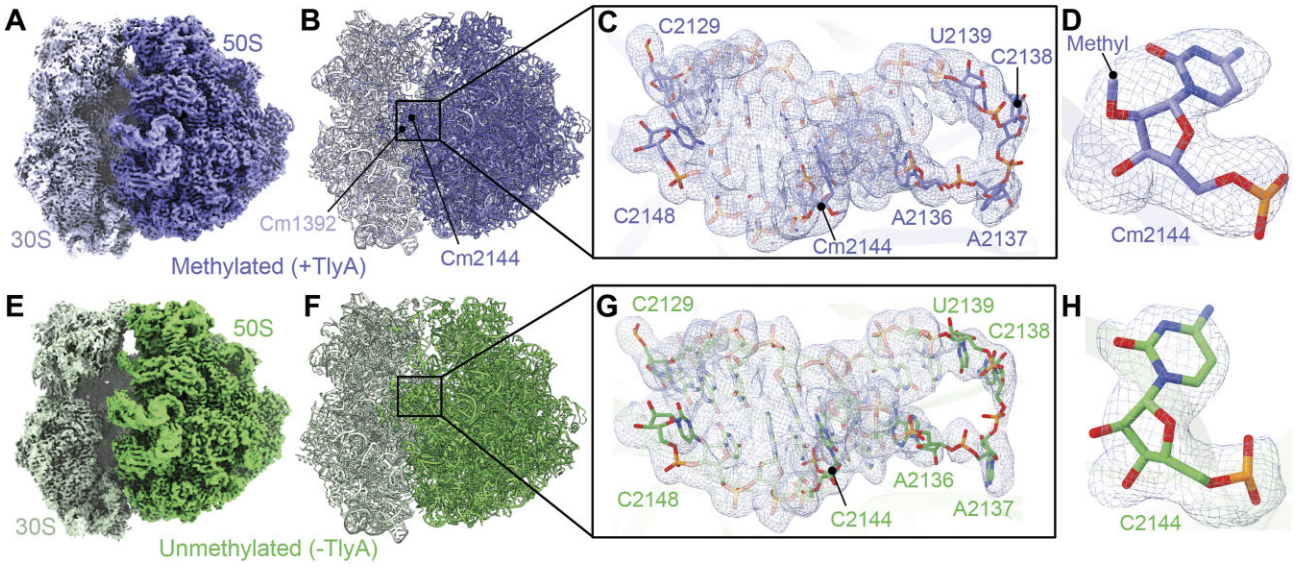

Figure 1. Cryo-EM map and model of the TlyA-methylated and unmethylated H69 within the *Msm* 70S ribosome. (**A**) Postprocessed (PHENIX sharpened) map of the methylated 70S ribosome at 3.16 Å resolution. (**B**) The final model highlighting the location of H69 (boxed region) and indicating the sites of methylation on both subunits. (**C**) Zoomed-in view of the indicated region, showing the H69 structure with a surrounding map from 50S multibody refinement (DeepEMhancer sharpened, map threshold 0.01; map value range −0.00171 to 1.86). (**D**) Methylated Cm2144 shown within the map (DeepEMhancer sharpened, map threshold 0.04; map value range −0.00171 to 1.86) supporting the presence of the expected 2′-*O*-methyl group. (**E**–**H**) As for panels (A)–(D) but for the unmethylated *Msm* 70S ribosome at 3.24 Å resolution, with the unmodified H69 (C2144) highlighted (boxed region). For panels (G) and (H), the map is DeepEMhancer sharpened with a map threshold of 0.013 and 0.042, respectively; map value range −0.00235 to 2.04.

through electrostatic and van der Waals interaction energy calculations between capreomycin and the RNA. RMSF values are averages from the three replicate simulations, while inter-residue angles and binding energy metrics were derived from the concatenated data. For System 2, RMSD (root-mean-square deviation)-based clustering was performed on each trajectory with 1-ns intervals on all non-hydrogen (heavy) atoms. The top 5–7 frames, covering over 60% of all conformations, were selected for RNA helical parameter analysis.

Calculation of H69 helical (base step) parameters

RNA helical parameters were calculated using the Web 3DNA 2.0 server [33] for H69 extracted from 70S ribosome structures LR222 (TlyA methylated), LR222 C101A (unmethylated), PDB code 5O61 (*Msm*), and PDB code 7TTU (*S. aureus*), or from H69 MD simulations (System 2). Values for six base step parameters (roll, shift, twist, slide, rise, and tilt) were plotted using GraphPad Prism 10 as comparisons for pairs of structures or as the difference in parameter value for H69 in our methylated and unmethylated 70S ribosome structures. Additionally, to assess trends in H69 helical parameter differences between these two structures, absolute values of each parameter difference were normalized, and the six normalized values were plotted together for each base step in GraphPad Prism 10. The same procedure was used for methylated and unmethylated H69 from MD simulations (System 2).

Results

Structures of TlyA^{II}-methylated and unmethylated *Msm* 70S ribosomes

Structures of the *Msm* 70S ribosome with and without the two TlyA-incorporated methylations were determined by single-particle cryo-EM at overall resolutions of 3.16 and 3.24 Å, respectively (Fig. 1). Multibody refinement resulted in similar overall resolution maps for the 50S and 30S subunit regions with slight improvement for the 50S subunit: methylated 50S (3.08 Å) and 30S (3.19 Å) and unmethylated 50S (3.17 Å) and 30S (3.37 Å) subunits. More importantly, multibody refinement improved the map quality for the region corresponding to H69, with local resolution analysis revealing similar values for H69 as the majority of the corresponding full 50S subunit (Supplementary Fig. S3E and K). The maps from multibody refinement were subsequently postprocessed without sharpening and sharpened using PHENIX (adjusted surface area) [25] and DeepEMhancer [26], and the model was generated by PHENIX-based structural refinement (Supplementary Figs S1 and S2). Finally, the separate 50S and 30S models were combined to create complete structures of the methylated and unmethylated 70S ribosomes (Fig. 1 and Supplementary Figs S1 and S2).

The resulting models include the entire H69 with its terminal tip residues, A2136–U2139, that form a four-nucleotide RNA loop and comprise part of the capreomycin binding pocket (Fig. 1C and G). The modification of C2144 in the methylated, but not unmethylated, 70S ribosome could be visualized, and the 2′-*O*-methylated nucleotide confidently modeled (Fig. 1D and H). Overall, the methylated and unmethylated ribosome structures are essentially identical, with an RMSD of ∼0.7 Å over 4043 phosphate backbone atoms. Additionally, both structures possess the expected mycobacterial ribosome-specific protein and 23S rRNA expansions [14], with only the long H54a expansion exhibiting positional variability as previously observed [19]. Thus, our structures of TlyA^{II}-methylated (LR222) and unmethylated (LR222 C101A) ribosomes appear virtually identical to one another and prior structures, indicating that the modifications incorporated by TlyA^{II} do not induce large-scale changes in 70S ribosome.

Downloaded from https://academic.oup.com/nar/article/53/13/gkaf618/8192813 by Acquisitions Dept Serials user on 23 July 2025

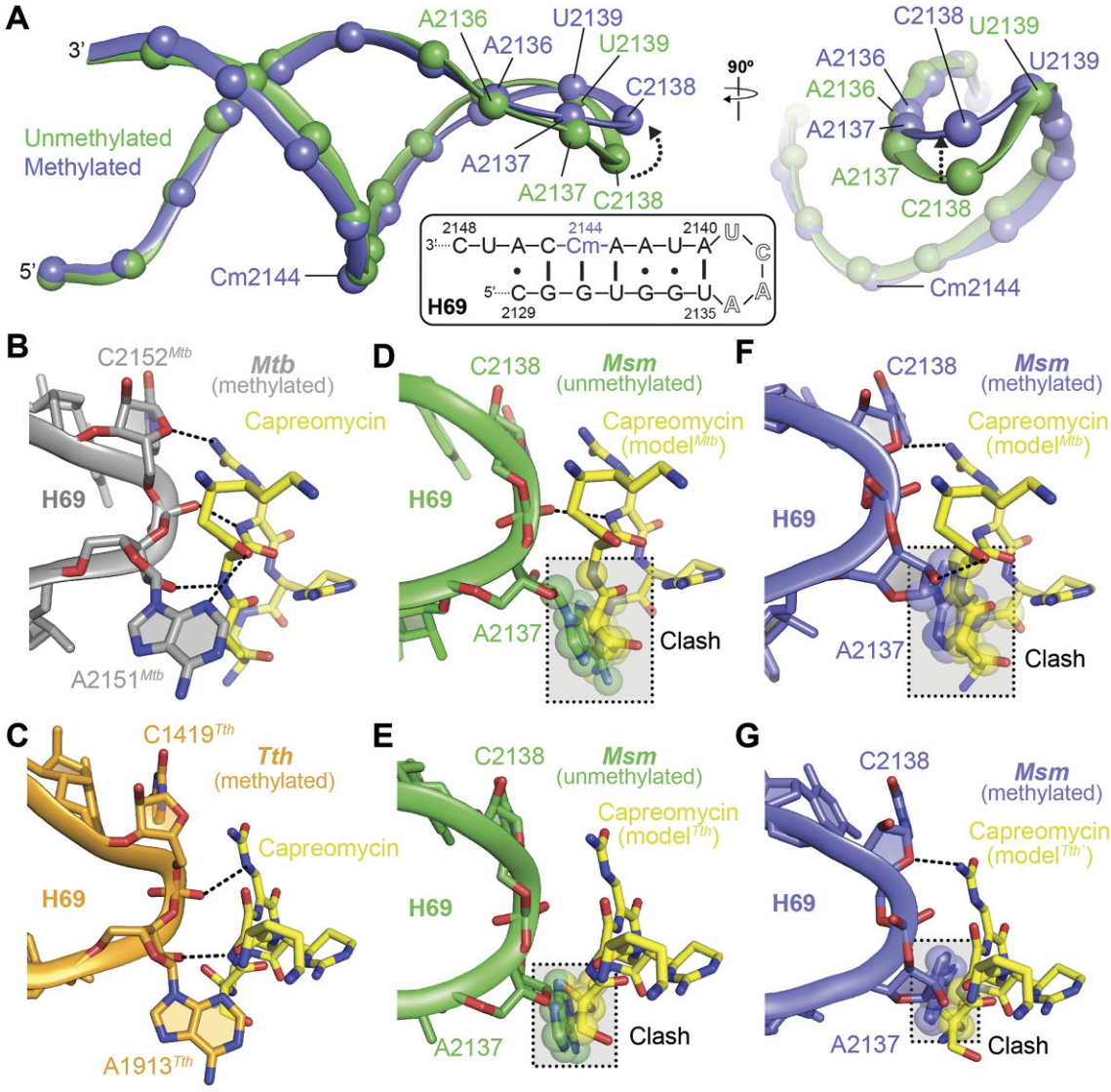

Figure 2. The nucleotides at the tip of H69 undergo changes in the methylated versus unmethylated ribosome, potentially impacting capreomycin binding. (**A**) Two orthogonal views of a superimposition of the methylated and unmethylated H69 shown as backbone with phosphates as spheres. Differences in the tip are indicated with a dotted line arrow. Inset: sequence and secondary structure of H69. (**B**) Residues A2151^{Mtb} and C2152^{Mtb} at the tip of H69 in the *Mtb* 70S ribosome (PDB code 5V93) stabilize capreomycin in its binding pocket via hydrogen bonding interactions (dashed lines). (**C**) Corresponding view for capreomycin at the H69 tip in the *Tth* 70S ribosome (PDB code 4V7M). (**D**, **E**) in the unmethylated *Msm* ribosome, A2137 is predicted to clash (boxed regions with atoms shown as semi-transparent spheres) with the modeled capreomycin from both the *Mtb* and *Tth* structures, respectively. In contrast, C2138 either weakly (*Mtb*) or does not interact (*Tth*) with the antibiotic. (**F**, **G**) in the methylated *Msm* ribosome, movement of C2138 and the tip of H69 partially opens the capreomycin binding pocket and allows the nucleotide to contact the modeled antibiotic. A2137 remains in a position predicted to result in clashes with the bound capreomycin and would thus require further movement promoted by drug binding as part of its mechanism of action in blocking tRNA (transfer RNA) movement.

C2144 2′-*O*-methylation results in a more open conformation of the tip of H69

Alignment of H69 from our methylated *Msm* 70S ribosome with that of a previously published *Msm* 70S structure (PDB code 5O61) reveals that these two H69 structures are very similar (Supplementary Fig. S4A and Supplementary Table S1). Likewise, a comparison of our unmethylated *Msm* ribosome and those from two bacteria lacking any TlyA, *L. innocua* (PDB code 8UU4) and *S. aureus* (PDB code 7TTU), reveals that H69 is structurally conserved among unmethylated ribosomes (Supplementary Fig. S4B and Supplementary Table S1). Direct comparison of H69 between our two new structures, with and without methylation by TlyA^{II}, reveals that the only significant difference is at the apical tip of the H69 helix (nucleotides A2136–U2139; Fig. 2A and Supplementary Table S1). In the methylated H69, the phosphodiester backbone shifts by ∼3 Å to create a more open conformation of these H69 loop nucleotides, whereas the corresponding region of the unmethylated ribosome adopts a more compact structure.

Nucleotides A2137 and C2138 at the tip of H69 have been reported to help anchor capreomycin in its binding pocket at the subunit interface [12, 13]. Therefore, to assess the potential effect of the structural differences observed in our structures at the tip of H69 on antibiotic binding, we compared our two structures with the *Mtb* and *Tth* 70S ribosome–

Downloaded from https://academic.oup.com/nar/article/53/13/gkaf618/8192813 by Acquisitions Dept Serials user on 23 July 2025

capreomycin complexes. Interestingly, all of H69 in these two drug-bound structures, including the phosphodiester backbone at the tip of the helix, is essentially identical to the unmethylated *Msm* 70S ribosome structure but with distinct orientations of the A2137 and C2138 nucleobases at the tip of H69 (Supplementary Fig. S4C and D), further supporting their role in positioning capreomycin (Fig. 2B and C).

Next, to compare our structures with those of capreomycin-bound *Mtb* and *Tth* H69, we modeled the antibiotic in the drug binding pocket within our methylated and unmethylated H69. The distinct orientations of A2137 and C2138 in the unmethylated *Msm* 70S H69 suggest that C2138 would make either no interactions or a single potential hydrogen bond with the modeled capreomycin from *Tth* and *Mtb*, respectively, while A2137 is positioned in a manner that would occlude drug binding in both cases (Fig. 2D and E, and Supplementary Fig. S5A). However, methylation of C2144, ~20 Å away from these nucleotides in H69, results in a reorientation of C2138 to a position more similar to that observed in the *Mtb* and *Tth* 70S ribosome structures, thus potentially restoring favorable interactions with capreomycin, including putative hydrogen bonds made by both the ribose and nucleobase of C2138 (Fig. 2F and G, and Supplementary Fig. S5B). These structures can thereby explain why the unmethylated H69 is less suitable for binding capreomycin, due to the loss of interactions made by C2138, resulting in the observed reduction in drug efficacy. In contrast, Cm2144 methylation positions C2138 to engage more favorably with capreomycin, which can support additional necessary reorganization (e.g. displacement of A2137) for full accommodation of the drug into its binding pocket. In further support of this idea, modeling capreomycin into either an *Mtb* 70S structure containing tRNAs and messenger RNA (mRNA) (PDB code 7MT7) or an isolated *Mtb* 50S subunit structure (PDB code 5V7Q), both determined without the drug, also reveals similar favorable interactions and clashes with nucleotides at H69 tip (Supplementary Fig. S4E and F). Thus, methylation of H69 itself, and not interactions with other ligands or between the subunits, appears to be the main driver of the reorganization of the H69 component of the capreomycin binding site.

Capreomycin binding to the methylated ribosome is enhanced by the altered H69 tip nucleotide geometry

To further explore the effect of H69 methylation on capreomycin binding, we performed partially restrained MD simulations of a section of the capreomycin-bound *Mtb* 70S ribosome (Fig. 3A), with and without the Cm2144 modification. Superimposition of the chosen *Mtb* 70S section on its equivalent in the methylated *Msm* 70S ribosome yields an RMSD of 1.0 Å over 117 phosphate atoms, highlighting the structural similarity in the two regions. In these simulations, no restraints were applied to capreomycin or H69 nucleotides, except for the two terminal base pairs (see the "Materials and methods" section for details). Comparison of RMSF values for the methylated and unmethylated systems shows that Cm2144 reduces the nucleotide dynamics of H69 compared to the unmethylated system between the site of modification and the tip of H69 (Fig. 3B). This stabilizing effect of Cm2144 on the H69 structure is also consistent with the lower *B*-factor for methylated (156.2 $Å^2$) compared to unmethylated (192.6 $Å^2$) H69 in our *Msm* 70S ribosome structures. Absence of the

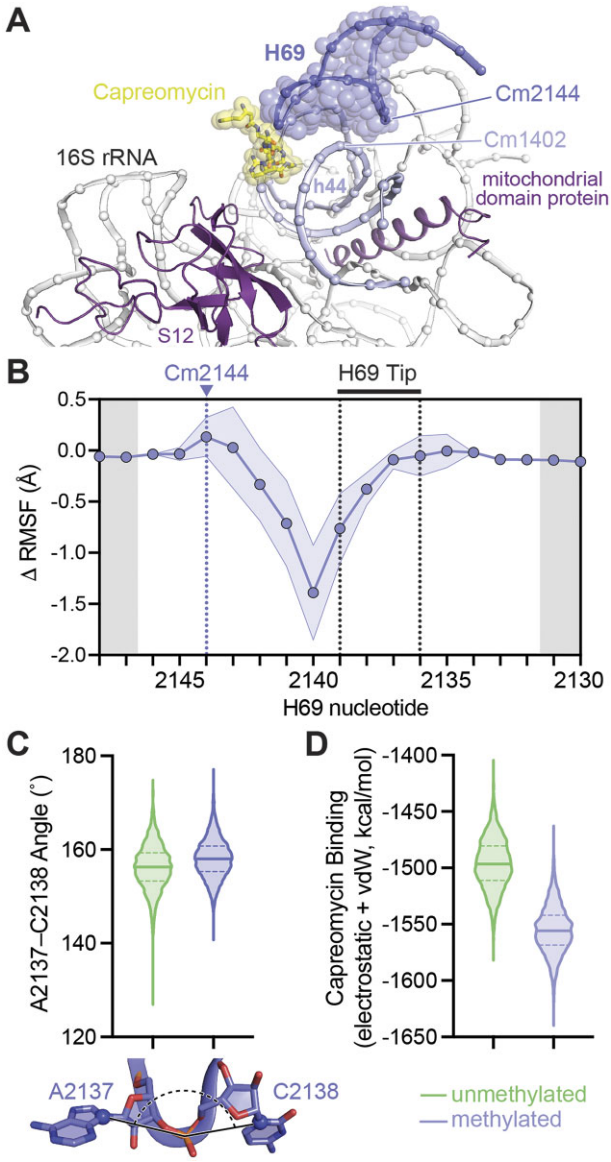

Figure 3. C2144 methylation stabilizes H69 and favors capreomycin binding. (**A**) The components of *Mtb* 70S ribosome (PDB code 5V93) used for MD simulation (System 1), including H69, h44 and additional 16S rRNA regions, ribosomal proteins, and capreomycin. The unrestrained regions are indicated with transparent spheres. Nucleotide positions are denoted by solid spheres (P atoms) on the rRNA ribbon. (**B**) Difference RMSF (unmethylated subtracted from methylated) for H69 reveals a decrease in dynamics between the site of modification (Cm2144) and the helix tip. The dotted lines indicate the site of methylation and the H69 tip, as indicated. The vertical shaded regions indicate the restrained regions of H69 and the standard deviation for calculated values is indicated by the shaded region surrounding the plotted data. (**C**) Plot showing the increase in average angle (indicated on the structure below the plot) between A2137 (N1) and C2138 (N9) in the methylated system compared to the unmethylated system. (**D**) Calculated capreomycin binding energy is more favorable (lower energy) in the methylated system compared to unmethylated.

methyl group also resulted in a decrease in the average angle between A2137 and C2138 in the simulation (Fig. 3C). These nucleotides at the tip of H69 are directly involved in capreomycin binding, further supporting the idea that the Cm2144 modification positions these distant nucleotides favorably for antibiotic binding. Finally, we observed an increase in calcu-

Downloaded from https://academic.oup.com/nar/article/53/13/gkaf618/8192813 by Acquisitions Dept Serials user on 23 July 2025

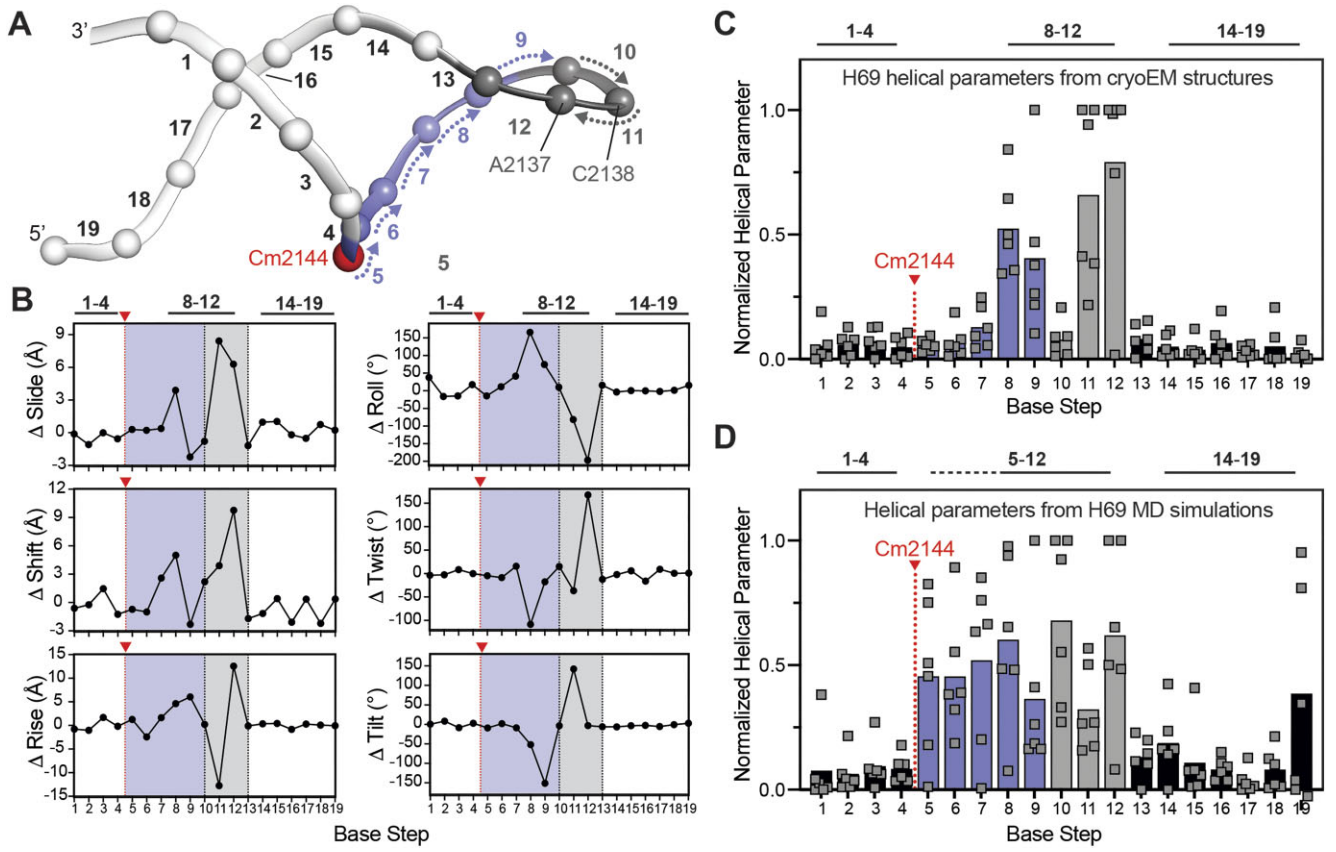

Figure 4. C2144 methylation results in propagation of helical conformational changes to the tip of H69. (**A**) H69 structure with the site of methylation and the two H69 tip residues critical for capreomycin binding indicated. Base steps for which helical parameters were calculated in 3DNA 2.0 and proposed direction of signal propagation (3′ to 5′) are also shown. (**B**) Differences between the indicated H69 helical parameters for methylated and unmethylated 70S ribosomes. The left dotted line, left shaded region, and right shaded region indicate the site of methylation (Cm2144), nucleotides between Cm2144 and the helix tip, and the H69 tip, respectively. (**C**) Comparison of the normalized differences between methylated and unmethylated H69 for the same six helical parameters at each base step. (**D**) As for panel (C) but from MD simulations of the methylated and unmethylated H69 structures (System 2). All individual helical parameter plots for methylated and unmethylated H69 are shown in Supplementary Fig. S6C and D.

lated capreomycin binding energy with rRNA in the unmethylated H69 compared to the methylated model, indicating that the absence of the modification reduces the binding affinity of the antibiotic (Fig. 3D). Overall, these MD simulations support the idea that H69 methylation at C2144 results in changes at the distant tip of the helix that favor capreomycin binding.

Allosteric propagation from Cm2144 results in the conformational change at the tip of H69

The site of methylation at C2144 is five nucleotides in the 3′ direction from U2139 (~23 Å distant), the final base of the four-nucleotide loop at the tip of H69. To understand how this distant methylation might influence the capreomycin binding pocket conformation, we analyzed RNA helical parameters for H69 nucleotides C2129–C2148, including the twist, roll, tilt, rise, slide, and shift of each nucleotide pair (i.e. base steps), which previous studies have shown to be useful in defining allosteric signaling in DNA [34, 35]. Comparison of the methylated (Cm2144) and unmethylated (C2144) H69 structures revealed differences in each of these helical parameters for the region comprising nucleotides U2141 to A2136, i.e. base steps 8–12 between the site of methylation at C2144 and A2136, the first 5′ nucleotide of the H69 loop (Fig. 4 and Supplementary Fig. S6A–C).

In contrast, no differences were observed in the other regions of the helix, i.e. for nucleotides U2135–C2129 of the complementary strand on the 5′ side of H69 (base steps 14–19) and nucleotides C2148–Cm2144 to the 3′ side of C2144 (base steps 1–4). We additionally compared the standard deviation for differences in each helical parameter averaged within each of these three distinct regions of H69. For all parameters assessed, these values were substantially higher for the region spanning from near the methylation site to U2139 (base steps 5–9), consistent with this region being the most impacted by the presence or absence of C2144 methylation (Supplementary Table S2). Finally, helical parameters were calculated for H69 from other structures of methylated *Msm* (PDB code 5O61) and unmethylated *S. aureus* (PDB code 7TTU) ribosomes and these were also found to be consistent with our methylated and unmethylated structures, respectively, with only minor differences primarily localized at the tip of the helix for the unmethylated structure (Supplementary Fig. S7A and B). These observations further support the idea that methylation triggers alterations in helical structure, ultimately facilitating allosteric signal transmission that propagates in the 3′ direction from C2144 to the H69 tip, resulting in the observed shifts in the loop nucleotide positions.

To further investigate how C2144 ribose methylation impacts conformational dynamics within H69 in the absence

Downloaded from https://academic.oup.com/nar/article/53/13/gkaf618/8192813 by Acquisitions Dept Serials user on 23 July 2025

of any influence from other ribosome regions, we performed MD simulations of H69 nucleotides C2129 to C2148 with and without the modification (System 2). To prevent unrealistic unpairing in this isolated model RNA system, nucleotides C2129–G2131 (base steps 18–19) and U2147–C2148 (base step 1) at the base of the H69 stem, which are normally connected to adjacent rRNA nucleotides in the 70S ribosome, were partially restrained during the simulations (see the "Materials and methods" section). Multiple conformations (five or more) of H69 from each simulation were selected using RMSD-based clustering of the trajectories, such that each set collectively represented >60% of all RNA conformations in the simulation. RNA helical parameters of these representative conformations were calculated, and the same six parameters compared as before (Fig. 4D and Supplementary Fig. S6D). Again, significant differences between methylated and unmethylated H69 were observed between the site of methylation and the nucleotides of the loop at the tip of H69 (base steps 5–12). Additionally, the H69 regions to both the 5′-(base steps 14–17) and 3′-side (base steps 1–4) remain essentially identical between the methylated and unmethylated ribosomes and exhibit significantly less variability between the representative structures from each simulation (indicated by the shaded region on each plot in Supplementary Fig. S6D). Thus, MD simulations further support the idea that methylation at C2144 imparts conformational and nucleotide dynamic changes on H69 that propagate exclusively from the site of modification back (3′ direction) to the tip of H69 where these changes manifest as allosteric alterations in the conformation of the capreomycin binding pocket.

16S rRNA C1392 methylation alters the conformation of the capreomycin binding pocket

Previously published structures of methylated *Mtb* and *Tth* 70S ribosomes with capreomycin showed that 16S rRNA nucleotide G1475 forms part of the drug binding site and directly interacts with the antibiotic [12, 13]. We next asked whether the TlyA^{II} methylations play a role in supporting the formation of this interaction with capreomycin but found no change in the position of G1475, which is similar in both our methylated and unmethylated structures and in the drug-bound structures (Supplementary Fig. S8). Thus, G1475 appears to be oriented to interact with the antibiotic regardless of the methylation status of 23S rRNA C2144 and 16S rRNA C1392.

16S rRNA nucleotide A1391 and the TlyA-target 16S rRNA nucleotide C1392 have also been proposed to be important for capreomycin binding as they are positioned to make potential weak hydrogen bonding interactions with the bound drug at the subunit interface [13, 16]. However, as these potential hydrogen-bonding interaction distances exceed ∼4.0 Å (Supplementary Fig. S9A and B), we asked whether these two 16S rRNA nucleotides might have an alternative role in supporting the formation of the capreomycin binding pocket. The 23S and 16S rRNA subunit interface in this region of our methylated and unmethylated ribosomes align with an RMSD of 0.86 Å to each other as well as to the interface of a previously reported *Mtb* 70S structure (PDB code 7MT7), indicating that they are overall structurally very similar (Supplementary Fig. S10A); however, local differences in H69 tip nucleotide positions are observed. In the unmethylated ribosome, C2138 at the tip of H69 interacts with C1392

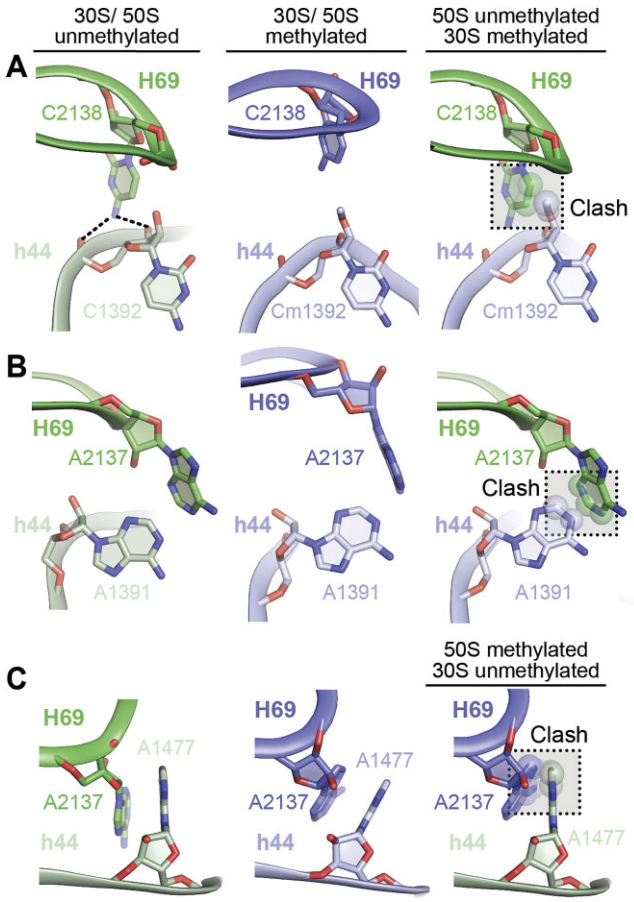

Figure 5. 16S rRNA nucleotides assist in preserving the architecture of the capreomycin binding site. (**A**) In the unmethylated ribosome (left), 23S rRNA C2138 interacts with 16S rRNA C1392, while in the methylated ribosome (center), these contacts are lost due to the movement of C2138 away from Cm1392. A model combining C2138 as positioned in the unmethylated ribosome and Cm1392 (right) shows that methylation would result in steric clashes (spheres) without this movement of C2138. Methylation of C1392 thus supports the maintenance of C2138 in the more open conformation of the H69 tip. (**B**) 16S rRNA A1391 and 23S rRNA A2137 are adjacent in the unmethylated ribosome but do not directly interact (left). In the methylated 70S ribosome (center), A2137 moves away from A1391 as the tip of H69 moves upward. A model combining A1391 in the methylated 30S reveals potential clashes with A2137 when positioned as observed in the more compact H69 conformation of the unmethylated 50S subunit (right). (**C**) In the unmethylated ribosome (left), 23S rRNA A2137 and 16S rRNA A1477 make a π-stacking interaction that is maintained by coordinated rotation of both nucleotides in the methylated ribosome (center). A model combining methylated 30S and unmethylated 50S subunits (right) shows steric clashes would result without the rotations, indicating that these movements maintain the stacking interaction and the more open conformation of H69 in the methylated ribosome.

of h44 (Fig. 5A, left, and Supplementary Fig. S5C), whereas in the methylated ribosome, since H69 becomes more open, C2138 packs further into its helix and thereby moves away from C1392, resulting in a loss of these interactions (Fig. 5A, center, and Supplementary Fig. S5D). Notably, without these reorientations, the methyl group of C1392 would clash with the base of C2138 (Fig. 5A, right). A similar clash is predicted using superimposition to model the interaction of unmethylated *Msm* H69 and methylated *Mtb* h44 (from PDB code 7MT7; Supplementary Fig. S10B), indicating that methylation of C1392 may directly contribute to maintaining the

Downloaded from https://academic.oup.com/nar/article/53/13/gkaf618/8192813 by Acquisitions Dept Serials user on 23 July 2025

more favorable position of C2138 for interaction with capreomycin. In contrast, A1391 is not positioned to form hydrogen bonds with A2137 in either the unmethylated or methylated ribosome, although the two nucleotides are closer in the methylated ribosome as compared to the unmethylated ribosome (Fig. 5B, left, and Supplementary Fig. S5C and D). However, A1391 in the context of TlyA^{II}-methylated h44 is slightly shifted toward A2137, while A2137 itself moves away from A1391, which ensures that potential steric clashes are avoided (Fig. 5B).

Finally, another significant movement was observed for the h44 strand complementary to the strand containing A1391 and C1392. In the unmethylated ribosome, the nucleobase of A1477 of h44 makes a π-stacking interaction with the nucleobase of A2137 in the H69 tip (Fig. 5C, left, and Supplementary Fig. S5A and E). This contact is preserved in the methylated ribosome through rotations of A2137 and A1477, the absence of which would result in steric clash (Fig. 5C and Supplementary Fig. S5B and F). Modeling the H69–h44 interface comprising the methylated *Mtb* H69 (PDB code 7MT7) and unmethylated *Msm* h44 reveals a similar predicted clash between the two nucleotides, highlighting the importance of the nucleotide rotations (Supplementary Fig. S10C). Additionally, previously published ribosome structures from different organisms, including *Eco* [36] and *Tth* [37, 38], also show the presence of the stacking interaction between A2137 and A1477, indicating its conservation across different species. Therefore, our structures suggest that the methylation of h44 alters the positions and interactions of C1392, A1391, and A1477 in a manner that supports the maintenance of changes at the tip of H69, allosterically mediated by C2144 methylation, that are necessary for optimal capreomycin binding and antimicrobial activity.

Discussion

We determined cryo-EM structures of two empty *Msm* 70S ribosomes that are identical except for the presence or absence of the two cytidine-2′-*O*-methylations incorporated by the methyltransferase TlyA^{II}. Thus, although the *Msm* ribosomes in our structures lack mRNA and tRNAs that would normally be present in the cell, this defined experimental system enabled us to determine the specific contributions of rRNA methylation to formation of the optimal tuberactinomycin drug binding pocket. Although the two structures are highly similar overall, they reveal key conformational differences at the tip of H69 of the 50S subunit and reorganization of key residues in h44 of the 30S subunit that depend on the presence or absence of the two modifications. This work thus reveals how rRNA methylation can promote ribosome-targeting drug activity, in contrast to the more widespread mechanism of blocking antibiotic binding by steric clashes that then lead to resistance [2, 39, 40]. In particular, we find that the more distant 23S rRNA methylation at C2144 causes conformational changes at the capreomycin drug binding site that, with additional reorganization of 16S rRNA nucleotides and a potential Cm1392 methylation-induced steric clash, all contribute to facilitating rather than impeding antibiotic binding. These changes appear to collectively underpin the observed rRNA methylation-dependent activity of tuberactinomycin antibiotics such as capreomycin.

Nucleotides A2137 and C2138 at the tip of H69 adopt distinct positions in previously published structures of methylated *Mtb* or *Tth* 70S with bound capreomycin [12, 13] as well as in the methylated and unmethylated *Msm* 70S structures presented here. In the unmethylated *Msm* ribosome, the tip of H69 adopts a more compact conformation, and is positioned close to h44 with A2137 and C2138 occupying the capreomycin binding pocket, presenting a steric hindrance to its binding (Fig. 6A). In the TlyA^{II}-methylated ribosome, the tip of H69 adopts a more open conformation in which C2138 moves away from h44 compared to the unmethylated ribosome. This reconfiguration opens up the capreomycin binding pocket in the assembled 70S ribosome and positions C2138 to anchor the incoming antibiotic (Fig. 6A). Therefore, the previously reported elevated capreomycin minimal inhibitory concentration (MIC) against *Eco* (which lacks TlyA) [11] and the appearance of clinical capreomycin-resistant isolates with *tlyA* mutations that render the enzyme inactive [41, 42] may be due to the lack of interactions between C2138 and capreomycin that support drug binding. TlyA-mediated methylation of C2144 brings C2138 closer to the antibiotic, promoting the drug–ribosome interaction and resulting in increased efficacy and the observed reduction in capreomycin MIC [11]. These structural observations were also corroborated by MD simulations that showed a decrease in the angle between A2137 and C2138 in the absence of methylation and a corresponding decrease in calculated capreomycin binding affinity. Interestingly, in our methylated *Msm* 70S ribosome structure and an *Mtb* 70S structure with tRNAs and mRNA (PDB code 7MT7), A2137 remains in a position that partially blocks the antibiotic binding site. In contrast, the structures of the *Mtb* and *Tth* 70S ribosome–capreomycin complexes show the same flipped orientation of this nucleotide that promotes its interaction with the A-site tRNA [13]. Thus, the need for capreomycin binding to trigger movement of A2137 from its position in the drug-free binding pocket may underpin the mechanism of drug action by promoting this nucleotide's interaction with the A-site tRNA, resulting in decoding defects and/or inhibition of translocation [15, 43].

Allosteric regulation of ribosome function can occur in response to antibiotic binding. For example, macrolide binding at the peptidyl transferase center enables sensing of leader peptide sequences traversing the nascent peptide exit tunnel and allosterically alters surrounding nucleotides to cause ribosome stalling for expression of macrolide-resistance genes [44, 45]. In contrast, less is known about how RNA modifications facilitate antibiotic binding, as in the case of the methylations incorporated by TlyA. Recent computational studies on allosteric coupling of different ribosome regions also reveal that H69, particularly 23S rRNA nucleotides A2136 and U2141, serves as an allosteric link between the 50S and 30S subunits [46]. Building on and consistent with this theme, our MD analyses revealed reduced nucleotide dynamics in the modified H69 and conformational changes beginning at the site of the ribose methylation at C2144 and propagating to the H69 tip (C2144 to A2136), which forms part of the capreomycin binding site located at the subunit interface. No other significant conformational changes occur upon methylation of H69, suggesting that this pathway is highly specific. The H69 conformational changes induced by methylation at C2144 are also clinically relevant because *Mtb* clinical isolates containing an A2140 deletion within H69 increase resistance to capreomycin [8]. The A2140 deletion also results in loss of the C2144 methylation, and together these changes increase the capreomycin MIC by >16-fold in *Msm*. Interestingly, the re-

Downloaded from https://academic.oup.com/nar/article/53/13/gkaf618/8192813 by Acquisitions Dept Serials user on 23 July 2025

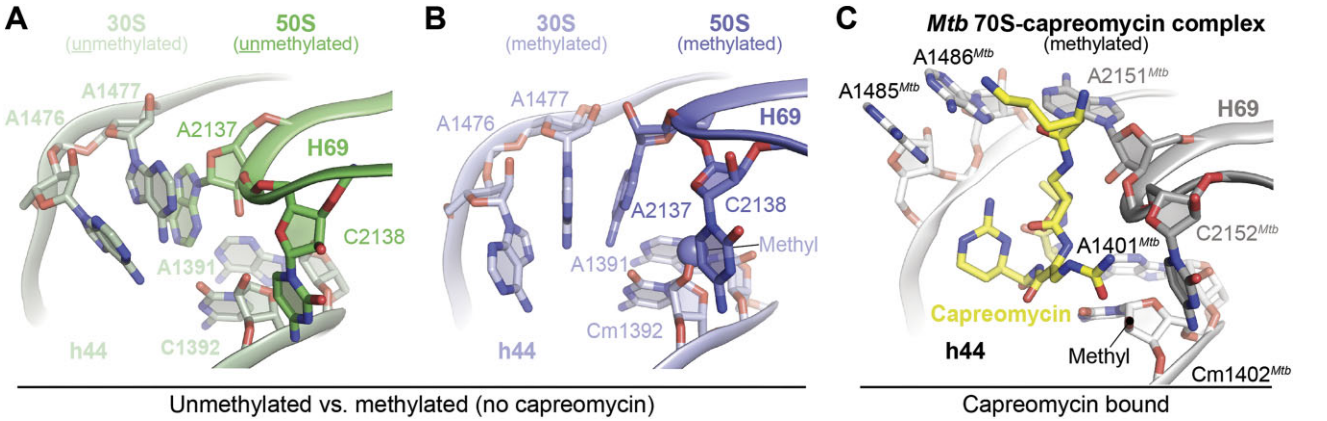

Figure 6. The capreomycin binding pocket formation is initiated by methylation and completed by antibiotic binding. (**A**) The tip of H69 in unmethylated *Msm* constituted by A2137 and C2138 is proximal to h44 residues C1392 and A1391. A2137 occupies the capreomycin binding pocket and C2138 is unfavorably positioned with respect to an incoming capreomycin antibiotic, reducing its affinity for the ribosome. (**B**) TlyA-mediated methylation of the 50S results in the transmission of an allosteric signal to the H69 tip, promoting a more open conformation. Within the assembled 70S ribosome, this conformation is preserved by the methyl group of 16S rRNA nucleotide C1392 (shown as a sphere) and the base of A1391. Rotation of A1477 compared to the unmethylated ribosome is also necessary to avoid clashes and thereby assists in maintaining the open conformation. (**C**) Upon capreomycin binding to the *M. tuberculosis* 70S ribosome (PDB code 5V93), A2151^{Mtb} (A2137) flips out of the binding pocket concurrent with a slight rotation of C2152^{Mtb} (C2138) in H69. h44 nucleotide A1485^{Mtb} (A1476) and A1486^{Mtb} (A1477) flip from the antibiotic binding site to accommodate the bound capreomycin. Note that although *Mtb* has active TlyA^{II}, the methyl group on Cm1402^{Mtb} was not modeled (location is indicated by "Methyl").

duction in susceptibility to capreomycin upon A2140 deletion alone is more pronounced than for loss of TlyA alone, suggesting that restricting the conformational plasticity of H69 impacts capreomycin binding to a larger extent. The importance of A2140 is consistent with helical analyses from our cryo-EM structures and MD simulations in which this nucleotide is consistently adjacent to the sites of major differences between methylated and unmethylated ribosomes (i.e. base steps 8 and 9 within the 8–12 region; Fig. 4). Together, these data suggest that A2140 may be a focal point in the allosteric relay of information from the site at C2144 and the tip of H69 that is critical for optimal capreomycin activity.

Although no large conformational changes are induced upon methylation of C1392 on the 30S subunit, our analyses provide evidence that this second TlyA^{II} modification may play a supporting role in promoting optimal tuberactinomycin activity. First, in the presence of capreomycin, an *Eco* strain expressing a TlyA^{II} variant that only partially methylates C1392 outcompeted a corresponding strain that fully modifies this site [11]. Second, identification of 16S rRNA mutations in *Mtb* clinical isolates and the finding that corresponding strains of *Msm* (A1391G and C1392U) have capreomycin sensitivities that are decreased by 8- to 16-fold, respectively [16, 47], further support the idea that, while H69 Cm2144 is of primary importance in terms of drug binding pocket formation, Cm1392 is also needed for full capreomycin activity.

Since both the Cm1392 and Cm2144 modifications are catalyzed by TlyA^{II} only in the context of the individual 30S and 50S subunits [11], the Cm1392 modification may help maintain the accessibility of the capreomycin binding pocket in its open conformation during the assembly of the 30S and 50S into a competent 70S complex. Additionally, some local conformational changes in adjacent nucleotides on the complementary strand are observed. Normally, the nucleobases of 23S rRNA A2137 at the tip of the methylated H69 and 16S rRNA A1477 form stacking interactions in the context of the 70S ribosome. Upon C1392 methylation, these two nucleotides would clash but the open conformation of H69 appears to reorganize this interaction to maintain stacking (Fig. 5C). This coordinated conformational change thus ensures maintenance of the h44–H69 interaction and, as a result, the open conformation of the H69 tip [36, 38]. Comparison of the Cm1392 and A1391 positions in the unmethylated and methylated *Msm* ribosomes with the corresponding residues in *Mtb* 70S shows considerable conservation of their interactions in each structure (Fig. 6A and B). This structural conservation contrasts with the process of the pocket formation by A2137 and C2138, where methylation and subsequently capreomycin binding affect the orientation of both these H69 tip residues. We thus propose that H69 methylation generates the open conformation of the capreomycin binding pocket, and h44 methylation ensures that this conformation remains open after the 50S and 30S subunits assemble to form the 70S. Finally, the nature of the capreomycin-bound state of h44 can be observed from the structure of the *Mtb* 70S ribosome–capreomycin complex, in which the residues A1476 (A1485^{Mtb}) and A1477 (A1486^{Mtb}) flip from the h44 RNA helix, in addition to the displacement of H69 nucleotide A2137 (A2151^{Mtb}) discussed above, to accommodate and interact with capreomycin (Fig. 6C, Supplementary Fig. S6C and F, and Supplementary Movie S1).

Although not directly addressed by the current work, why some bacterial species such as mycobacteria maintain TlyA and the modification(s) it incorporates is an interesting question given the impact on fitness under tuberactinomycin antibiotic stress. Indeed, some studies on growth of *Msm* strains with and without TlyA have reported no distinguishable difference in their generation times [10, 11]. However, loss of *tlyA* has been shown to slow growth of *Msm* strains with a mutation at A1408 (commonly observed in *Mtb* clinical isolates), suggesting that there is a fitness impact in these mutated *Mtb* strains [47]. Interestingly, a previous study has also indicated that Cm2144 is important for bacterial translation

Downloaded from https://academic.oup.com/nar/article/53/13/gkaf618/8192813 by Acquisitions Dept Serials user on 23 July 2025

at some temperatures by altering the strength of the contacts between the 50S and 30S subunits [48]. Further, other homologs of TlyA have recently been shown to play an important role in translation with deletion of *B. subtilis* TlyA [49] or *C. jejuni* Cj0588 [50] resulting in a temperature-dependent defect in ribosome formation (increased 50S and decreased 70S). These studies, and our finding that Cm2144 methylation appears to fine-tune H69 conformation and dynamics, suggest that maintaining TlyA is favorable under some conditions, but such benefits are outweighed under tuberactinomycin antibiotic stress.

Overall, our findings elucidate the necessity of a distant ribose methylation for capreomycin binding and highlight the importance of a previously unappreciated pathway of allosteric signaling within 23S rRNA H69. Although capreomycin has a long history of use as an anti-TB agent, it has recently been excluded by the WHO due to its poor performance compared to other current treatments [51]. However, efforts are underway to explore combination therapies of capreomycin with other drugs [52], and future targeting of the tuberactinomycin binding site with new generations of antimicrobials may prove fruitful in developing much needed treatments for multidrug-resistant TB. The role of distant methylation-mediated changes in antibiotic binding sites such as those revealed here may thus represent an important new consideration for designing more effective small molecules targeting the bacterial ribosome.

Acknowledgements

We thank Dr James Posey and colleagues at the Centers for Disease Control and Prevention, Atlanta, GA, for providing *M. smegmatis* strains (LR222 and LR222 C101A), Dr Ravi K. Koripella for assistance in specimen preparation for cryo-EM, and the staff at the National Center for CryoEM Access and Training (NCCAT) for high-resolution data collection.

Author contributions: Suparno Nandi (Investigation [lead], Writing—original draft [lead], Writing—review & editing [equal]), Debayan Dey (Conceptualization [supporting], Investigation [supporting], Writing—review & editing [supporting]), Pooja Srinivas (Investigation [supporting], Writing—review & editing [supporting]), Christine M. Dunham (Conceptualization [supporting], Funding acquisition [lead], Writing—review & editing [supporting]), and Graeme L Conn (Conceptualization [lead], Funding acquisition [lead], Writing—review & editing [equal]).

Supplementary data

Supplementary data is available at NAR online.

Conflict of interest

None declared.

Funding

This work was supported by the National Institutes of Health (R01-AI088025 to G.L.C. and C.M.D., and T32-GM008602 and T32-AI106699 to P.S.). C.M.D. is a Burroughs Wellcome Fund Investigator in the Pathogenesis of Infectious Disease. Some of this work was performed at the National Center for CryoEM Access and Training (NCCAT) and the Simons Electron Microscopy Center located at the New York Structural Biology Center, supported by the NIH Common Fund Transformative High Resolution Cryo-Electron Microscopy program (U24 GM129539) and by grants from the Simons Foundation (SF349247) and NY State Assembly. This work also benefitted from access to resources in the Emory University Robert P. Apkarian Integrated Electron Microscopy Core Facility (RRID:SCR_023537). Funding to pay the Open Access publication charges for this article was provided by National Institutes of Health.

Data availability

Structural coordinates for the TlyA-methylated and unmethylated 70S ribosomes have been deposited in the Protein Data Bank (PDB) with accession codes 9E0P and 9E0N, respectively. Corresponding cryo-EM maps have been deposited in the Electron Microscopy Data Bank (EMDB): 47365 and 47363.

References

1. Polikanov YS, Aleksashin NA, Beckert B *et al.* The mechanisms of action of ribosome-targeting peptide antibiotics. *Front Mol Biosci* 2018;**5**:48. https://doi.org/10.3389/fmolb.2018.00048
2. Jeremia L, Deprez BE, Dey D *et al.* Ribosome-targeting antibiotics and resistance via ribosomal RNA methylation. *RSC Med Chem* 2023;**14**:624–43. https://doi.org/10.1039/D2MD00459C
3. Cox G, Ejim L, Stogios PJ *et al.* Plazomicin retains antibiotic activity against most aminoglycoside modifying enzymes. *ACS Infect Dis* 2018;**4**:980–7. https://doi.org/10.1021/acsinfecdis.8b00001
4. Gaynor M, Mankin AS. Macrolide antibiotics: binding site, mechanism of action, resistance. *Curr Top Med Chem* 2003;**3**:949–61. https://doi.org/10.2174/1568026033452159
5. Wachino JI, Doi Y, Arakawa Y. Aminoglycoside resistance: updates with a focus on acquired 16S ribosomal RNA methyltransferases. *Infect Dis Clin North Am* 2020;**34**:887–902. https://doi.org/10.1016/j.idc.2020.06.002
6. Zou J, Zhang W, Zhang H *et al.* Studies on aminoglycoside susceptibility identify a novel function of KsgA to secure translational fidelity during antibiotic stress. *Antimicrob Agents Chemother* 2018;**62**:e00853-18 https://doi.org/10.1128/AAC.00853-18
7. Nishimura K, Hosaka T, Tokuyama S *et al.* Mutations in *rsmG*, encoding a 16S rRNA methyltransferase, result in low-level streptomycin resistance and antibiotic overproduction in *Streptomyces coelicolor* A3(2). *J Bacteriol* 2007;**189**:3876–83. https://doi.org/10.1128/JB.01776-06
8. Johansen SK, Maus CE, Plikaytis BB *et al.* Capreomycin binds across the ribosomal subunit interface using tlyA-encoded 2′-*O*-methylations in 16S and 23S rRNAs. *Mol Cell* 2006;**23**:173–82. https://doi.org/10.1016/j.molcel.2006.05.044
9. World Health Organization. *Global Tuberculosis Report 2019*. Geneva: World Health Organization, 2019.
10. Maus CE, Plikaytis BB, Shinnick TM. Mutation of tlyA confers capreomycin resistance in *Mycobacterium tuberculosis*. *Antimicrob Agents Chemother* 2005;**49**:571–7. https://doi.org/10.1128/AAC.49.2.571-577.2005
11. Monshupanee T, Johansen SK, Dahlberg AE *et al.* Capreomycin susceptibility is increased by TlyA-directed 2′-*O*-methylation on both ribosomal subunits. *Mol Microbiol* 2012;**85**:1194–203. https://doi.org/10.1111/j.1365-2958.2012.08168.x
12. Yang K, Chang JY, Cui Z *et al.* Structural insights into species-specific features of the ribosome from the human pathogen *Mycobacterium tuberculosis*. *Nucleic Acids Res* 2017;**45**:10884–94. https://doi.org/10.1093/nar/gkx785

Downloaded from https://academic.oup.com/nar/article/53/13/gkaf618/8192813 by Acquisitions Dept Serials user on 23 July 2025

13. Stanley RE, Blaha G, Grodzicki RL *et al.* The structures of the anti-tuberculosis antibiotics viomycin and capreomycin bound to the 70S ribosome. *Nat Struct Mol Biol* 2010;**17**:289–93. https://doi.org/10.1038/nsmb.1755
14. Hentschel J, Burnside C, Mignot I *et al.* The complete structure of the *Mycobacterium smegmatis* 70S ribosome. *Cell Rep* 2017;**20**:149–60. https://doi.org/10.1016/j.celrep.2017.06.029
15. Szaflarski W, Vesper O, Teraoka Y *et al.* New features of the ribosome and ribosomal inhibitors: non-enzymatic recycling, misreading and back-translocation. *J Mol Biol* 2008;**380**:193–205. https://doi.org/10.1016/j.jmb.2008.04.060
16. Akbergenov R, Shcherbakov D, Matt T *et al.* Molecular basis for the selectivity of antituberculosis compounds capreomycin and viomycin. *Antimicrob Agents Chemother* 2011;**55**:4712–7. https://doi.org/10.1128/AAC.00628-11
17. Perlaza-Jimenez L, Tan KS, Piper SJ *et al.* A structurally characterized *Staphylococcus aureus* evolutionary escape route from treatment with the antibiotic linezolid. *Microbiol Spectr* 2022;**10**:e0058322. https://doi.org/10.1128/spectrum.00583-22
18. Seely SM, Basu RS, Gagnon MG. Mechanistic insights into the alternative ribosome recycling by HflXr. *Nucleic Acids Res* 2024;**52**:4053–66. https://doi.org/10.1093/nar/gkae128
19. Laughlin ZT, Nandi S, Dey D *et al.* 50S subunit recognition and modification by the *Mycobacterium tuberculosis* ribosomal RNA methyltransferase TlyA. *Proc Natl Acad Sci USA* 2022;**119**:e2120352119. https://doi.org/10.1073/pnas.2120352119
20. Li Z, Ge X, Zhang Y *et al.* Cryo-EM structure of *Mycobacterium smegmatis* ribosome reveals two unidentified ribosomal proteins close to the functional centers. *Protein Cell* 2018;**9**:384–8.
21. Suloway C, Pulokas J, Fellmann D *et al.* Automated molecular microscopy: the new Leginon system. *J Struct Biol* 2005;**151**:41–60. https://doi.org/10.1016/j.jsb.2005.03.010
22. Scheres SH. RELION: implementation of a Bayesian approach to cryo-EM structure determination. *J Struct Biol* 2012;**180**:519–30. https://doi.org/10.1016/j.jsb.2012.09.006
23. Zhang K. Gctf: real-time CTF determination and correction. *J Struct Biol* 2016;**193**:1–12. https://doi.org/10.1016/j.jsb.2015.11.003
24. Nakane T, Kimanius D, Lindahl E *et al.* Characterisation of molecular motions in cryo-EM single-particle data by multi-body refinement in RELION. *eLife* 2018;**7**:e36861. https://doi.org/10.7554/eLife.36861
25. Terwilliger TC, Sobolev OV, Afonine PV *et al.* Automated map sharpening by maximization of detail and connectivity. *Acta Crystallogr D Struct Biol* 2018;**74**:545–59. https://doi.org/10.1107/S2059798318004655
26. Sanchez-Garcia R, Gomez-Blanco J, Cuervo A *et al.* DeepEMhancer: a deep learning solution for cryo-EM volume post-processing. *Commun Biol* 2021;**4**:874. https://doi.org/10.1038/s42003-021-02399-1
27. Adams PD, Afonine PV, Bunkoczi G *et al.* PHENIX: a comprehensive Python-based system for macromolecular structure solution. *Acta Crystallogr D Biol Crystallogr* 2010;**66**:213–21. https://doi.org/10.1107/S0907444909052925
28. Pettersen EF, Goddard TD, Huang CC *et al.* UCSF Chimera—a visualization system for exploratory research and analysis. *J Comput Chem* 2004;**25**:1605–12. https://doi.org/10.1002/jcc.20084
29. Emsley P, Lohkamp B, Scott WG *et al.* Features and development of Coot. *Acta Crystallogr D Biol Crystallogr* 2010;**66**:486–501. https://doi.org/10.1107/S0907444910007493
30. Delano W. PyMOL: an open-source molecular graphics tool. *CCP4 Newsletter Pro Crystallogr* 2002;**40**:82–92.
31. Pettersen EF, Goddard TD, Huang CC *et al.* UCSF ChimeraX: structure visualization for researchers, educators, and developers. *Protein Sci* 2021;**30**:70–82. https://doi.org/10.1002/pro.3943
32. Panecka J, Mura C, Trylska J. Interplay of the bacterial ribosomal A-site, S12 protein mutations and paromomycin binding: a molecular dynamics study. *PLoS One* 2014;**9**:e111811. https://doi.org/10.1371/journal.pone.0111811
33. Li S, Olson WK, Lu XJ. Web 3DNA 2.0 for the analysis, visualization, and modeling of 3D nucleic acid structures. *Nucleic Acids Res* 2019;**47**:W26–34. https://doi.org/10.1093/nar/gkz394
34. Drsata T, Zgarbova M, Jurecka P *et al.* On the use of molecular dynamics simulations for probing allostery through DNA. *Biophys J* 2016;**110**:874–6. https://doi.org/10.1016/j.bpj.2015.12.039
35. Drsata T, Zgarbova M, Spackova N *et al.* Mechanical model of DNA allostery. *J Phys Chem Lett* 2014;**5**:3831–5. https://doi.org/10.1021/jz501826q
36. Fu Z, Indrisiunaite G, Kaledhonkar S *et al.* The structural basis for release-factor activation during translation termination revealed by time-resolved cryogenic electron microscopy. *Nat Commun* 2019;**10**:2579. https://doi.org/10.1038/s41467-019-10608-z
37. Polikanov YS, Steitz TA, Innis CA. A proton wire to couple aminoacyl-tRNA accommodation and peptide-bond formation on the ribosome. *Nat Struct Mol Biol* 2014;**21**:787–93. https://doi.org/10.1038/nsmb.2871
38. Neubauer C, Gao YG, Andersen KR *et al.* The structural basis for mRNA recognition and cleavage by the ribosome-dependent endonuclease RelE. *Cell* 2009;**139**:1084–95. https://doi.org/10.1016/j.cell.2009.11.015
39. Svetlov MS, Syroegin EA, Aleksandrova EV *et al.* Structure of Erm-modified 70S ribosome reveals the mechanism of macrolide resistance. *Nat Chem Biol* 2021;**17**:412–20. https://doi.org/10.1038/s41589-020-00715-0
40. Osterman IA, Dontsova OA, Sergiev PV. rRNA methylation and antibiotic resistance. *Biochemistry* 2020;**85**:1335–49. https://doi.org/10.1134/S000629792011005X
41. Zhao J, Wei W, Yan H *et al.* Assessing capreomycin resistance on tlyA deficient and point mutation (G695A) *Mycobacterium tuberculosis* strains using multi-omics analysis. *Int J Med Microbiol* 2019;**309**:151323. https://doi.org/10.1016/j.ijmm.2019.06.003
42. Li Q, Gao H, Zhang Z *et al.* Mutation and transmission profiles of second-line drug resistance in clinical isolates of drug-resistant *Mycobacterium tuberculosis* from Hebei Province, China. *Front Microbiol* 2019;**10**:1838. https://doi.org/10.3389/fmicb.2019.01838
43. Moazed D, Noller HF. Chloramphenicol, erythromycin, carbomycin and vernamycin B protect overlapping sites in the peptidyl transferase region of 23S ribosomal RNA. *Biochimie* 1987;**69**:879–84. https://doi.org/10.1016/0300-9084(87)90215-X
44. Vazquez-Laslop N, Klepacki D, Mulhearn DC *et al.* Role of antibiotic ligand in nascent peptide-dependent ribosome stalling. *Proc Natl Acad Sci USA* 2011;**108**:10496–501. https://doi.org/10.1073/pnas.1103474108
45. Arenz S, Meydan S, Starosta AL *et al.* Drug sensing by the ribosome induces translational arrest via active site perturbation. *Mol Cell* 2014;**56**:446–52. https://doi.org/10.1016/j.molcel.2014.09.014
46. Walker AS, Russ WP, Ranganathan R *et al.* RNA sectors and allosteric function within the ribosome. *Proc Natl Acad Sci USA* 2020;**117**:19879–87. https://doi.org/10.1073/pnas.1909634117
47. Freihofer P, Akbergenov R, Teo Y *et al.* Nonmutational compensation of the fitness cost of antibiotic resistance in mycobacteria by overexpression of tlyA rRNA methylase. *RNA* 2016;**22**:1836–43. https://doi.org/10.1261/rna.057257.116
48. Polikanov YS, Melnikov SV, Soll D *et al.* Structural insights into the role of rRNA modifications in protein synthesis and ribosome assembly. *Nat Struct Mol Biol* 2015;**22**:342–4. https://doi.org/10.1038/nsmb.2992
49. Hibma JL, Munson LM, Jones JD *et al.* TlyA is a 23S and 16S 2′-*O*-methylcytidine methyltransferase important for ribosome assembly in *Bacillus subtilis*. bioRxiv, https://doi.org/10.1101/2025.04.21.649808, 25 April 2025, preprint: not peer reviewed.

Downloaded from https://academic.oup.com/nar/article/53/13/gkaf618/8192813 by Acquisitions Dept Serials user on 23 July 2025

50. Salamaszynska-Guz A, Taciak B, Kwiatek A *et al.* The Cj0588 protein is a *Campylobacter jejuni* RNA methyltransferase. *Biochem Biophys Res Commun* 2014;**448**:298–302. https://doi.org/10.1016/j.bbrc.2014.04.104
51. Migliori GB, Tiberi S. WHO drug-resistant TB guidelines 2022: what is new? *Int J Tuberc Lung Dis* 2022;**26**:590–1. https://doi.org/10.5588/ijtld.22.0263
52. Shao Z, Chow MYT, Chow SF *et al.* Co-delivery of D-LAK antimicrobial peptide and capreomycin as inhaled powder formulation to combat drug-resistant tuberculosis. *Pharm Res* 2023;**40**:1073–86.

Downloaded from https://academic.oup.com/nar/article/53/13/gkaf618/8192813 by Acquisitions Dept Serials user on 23 July 2025

Received: November 5, 2024. **Revised:** May 23, 2025. **Editorial Decision:** June 11, 2025. **Accepted:** June 13, 2025
© The Author(s) 2025. Published by Oxford University Press on behalf of Nucleic Acids Research.
This is an Open Access article distributed under the terms of the Creative Commons Attribution-NonCommercial License (https://creativecommons.org/licenses/by-nc/4.0/), which permits non-commercial re-use, distribution, and reproduction in any medium, provided the original work is properly cited. For commercial re-use, please contact reprints@oup.com for reprints and translation rights for reprints. All other permissions can be obtained through our RightsLink service via the Permissions link on the article page on our site—for further information please contact journals.permissions@oup.com.